NPRL3 loss alters neuronal morphology, mTOR localization, cortical lamination, and seizure threshold

Philip H. Iffland II,[1] Mariah E. Everett,[2] Katherine M. Cobb-Pitstick,[3] Lauren E. Bowser,[2] Allan E. Barnes,[1] Janice K. Babus,[1] Andrea J. Romanowski,[1] Marianna Baybis,[1] Soad Elziny,[1] Erik G. Puffenberger,[2] Claudia Gonzaga-Jauregui,[4] Alexandros Poulopoulos,[1] Vincent J. Carson[2] and Peter B. Crino[1]

1 University of Maryland School of Medicine Departments of Neurology and Pharmacology, Baltimore, MD, 21201, USA

2 Clinic for Special Children, Strasburg, PA, 17579, USA

3 UPMC Children's Hospital of Pittsburgh Department of Neurology, Pittsburgh, PA, 15224, USA

4 Regeneron Genetics Center, Regeneron Pharmaceuticals Inc., Tarrytown, New York, 10591, USA

Correspondence to: Peter B. Crino, MD, PhD

Department of Neurology

University of Maryland School of Medicine

110 S. Paca St.

Baltimore, MD 21201, USA

E-mail: pcrino@som.umaryland.edu

Running title: NPRL3 loss and effects on brain function

Abstract

Mutations in nitrogen permease regulator-like 3 *(NPRL3)*, a component of the GATOR1 complex within the mechanistic target of rapamycin (mTOR) pathway, are associated with epilepsy and malformations of cortical development. Little is known about the effects of *NPRL3* loss on neuronal mTOR signaling and morphology, or cerebral cortical development and seizure susceptibility. We report the clinical phenotypic spectrum of a founder *NPRL3* pedigree (c.349delG, p.Glu117LysFS; n=133) among Old Order Mennonites dating to 1727. Next, as a strategy to define the role of NPRL3 in cortical development, CRISPR/Cas9 *Nprl3* knockout in Neuro2a cells *in vitro* and in fetal mouse brain *in vivo* was used to assess effects of *Nprl3* knockout on mTOR activation, subcellular mTOR localization, nutrient signaling, cell morphology and aggregation, cerebral cortical cytoarchitecture, and network integrity. The *NPRL3* pedigree exhibited an epilepsy penetrance of 28% and heterogeneous clinical phenotypes with a range of epilepsy semiologies i.e., focal or generalized onset, brain imaging abnormalities i.e., polymicrogyria, focal cortical dysplasia, or normal imaging, and EEG findings, e.g., focal, multi-focal, or generalized spikes, focal or generalized slowing. Whole exome analysis comparing a seizure-free group (n=37) to those with epilepsy (n=24) to search for gene modifiers for epilepsy did not identify a unique genetic modifier that explained the variability in seizure penetrance in this cohort. *Nprl3* knockout *in vitro* caused mTOR pathway hyperactivation, cell soma enlargement, and the formation of cellular aggregates seen in time-lapse videos that were prevented with the mTOR inhibitors rapamycin or torin1. In *Nprl3* KO cells, mTOR remained localized on the lysosome in a constitutively active conformation, as evidenced by phosphorylation of S6 and 4E-BP1 proteins, even under nutrient starvation (amino acid free) conditions, demonstrating that *Nprl3* loss decouples mTOR activation from neuronal metabolic state. To model human malformations of cortical development associated with *NPRL3* variants, we created a focal *Nprl3* KO in fetal mouse cortex by *in utero* electroporation and found altered cortical lamination and white matter heterotopic neurons, effects which were prevented with rapamycin treatment. EEG recordings showed network hyperexcitability and reduced seizure threshold to pentylenetetrazol treatment. *NPRL3* variants are linked to a highly variable clinical phenotype which we propose result from mTOR-dependent effects on cell structure, cortical development, and network organization.

Keywords: GATOR1; mTOR; cortical malformations; focal cortical dysplasia; epilepsy

Abbreviations: AAF = amino acid free; CFP = cyan fluorescent protein; CRISPR = clustered regularly interspaced short palindromic repeats; CTIP2 = COUP-TF-interacting protein 2; C:Y = CFP to YFP ratio; DEPDC5 = DEP-domain containing 5; DMSO = dimethyl sulfoxide; F-actin = filamentous actin; FCD = focal cortical dysplasia; FRET = fluorescence resonance energy transfer; GATOR1 = GTPase-activating protein activity towards rags complex 1; GFP = green fluorescent protein; gRNA = guide RNA; HME = hemimegalencephaly; IUE = in utero electroporation; KO = knockout; LAMP2 = lysosomal associated membrane protein 2; MAP2 = microtubule associated protein 2; MCD = malformation of cortical development; MPG = mTOR pathway gene; mTOR = mechanistic target of rapamycin; mTORC1/2 = mechanistic target of rapamycin complex 1/2; N2aC = neuro2a cells; NPRL2 = nitrogen permease regulator like-2; NPRL3 = nitrogen permease regulator like-3; P3 = postnatal day three; P4E-BP1 = phosphorylation of eukaryotic translation initiation factor 4E (elf4E)- binding protein-1; PFA = paraformaldehyde; PTZ = pentylenetetrazol; PS6 = phospho-ribosomal S6; RIPA buffer = radioimmunoprecipitation assay buffer; ROI = region of interest; RT = room temperature; S6 = ribosomal S6 protein; scram = scramble control; SEM = standard error of the mean; SUDEP = sudden unexplained death in epilepsy; TORCAR = mTORC1 activity reporter; WT = wildtype; YFP = yellow fluorescent protein

Introduction

Germline and somatic variants in mTOR pathway genes (MPG) are the most common causes of malformations of cortical development (MCD).[1] The mTOR pathway plays a pivotal role in cerebral cortical development[2] and MPG variants leading to constitutive mTOR activation ('mTORopathies') provide the presumed pathogenic mechanism for altered cortical cytoarchitecture. Focal cortical dysplasia II (FCDII) is a MCD highly associated with drug resistant seizures defined pathologically by disorganized cerebral cortical lamination, enlarged (cytomegalic) dysmorphic neurons, and heterotopic neurons in the white matter.[3] Variants in genes encoding components of the GTPase-Activating Protein (GAP)-Activity Towards Rags Complex 1 (GATOR1), including DEP-domain containing 5 (*DEPDC5*), Nitrogen Permease Regulator Like-2 (*NPRL2*), and Nitrogen Permease Regulator Like-3 (*NPRL3*)[4-6] are the most common MPG variants associated with FCDII[7] and hemimegalencephaly (HME), a MCD defined by hemispheric enlargement and FCDII histopathology. [8,9]

In non-neural cells, the GATOR1 complex modulates mTOR pathway activity in response to intracellular amino acid levels by governing translocation of mTORC1 (mTOR complex 1, mTOR bound to raptor) to and from the lysosomal membrane.[10,11] In nutrient replete conditions, GATOR1 is inhibited, releasing mTORC1 to physically interact with its binding partners on the lysosomal surface in an active conformation. However, when intracellular amino acids are low, GATOR1 prevents translocation of mTORC1 to the lysosomal surface (remaining cytoplasmic) thereby inhibiting mTOR activity.[12] GATOR1 subunits are highly expressed in brain[13,14] and the effects of, for example, *DEPDC5* variants on cell size, motility, firing, and cortical lamination have been assayed in experimental models[15-20] and human brain specimens.[4,7] While human tissue studies show a link between *NPRL3* variants, MCD, and mTOR activation,[7,15,21] few studies have investigated the role of *NPRL3* in neuronal morphology, cortical lamination, and cortical circuitry.

We report the largest and genealogically oldest known *NPRL3* patient pedigree and show that despite a common founder variant, clinical findings among affected individuals were highly heterogeneous with a spectrum ranging from normal brain imaging to HME and seizure freedom to drug resistant epilepsy. As a strategy to define mechanisms for clinical phenotypic heterogeneity, exome analysis was performed in this cohort but did not identify a gene modifier for seizure phenotype suggesting autonomous effects of the *NPRL3* variant. To assess the role of *NPRL3* in fetal brain development, CRISPR/Cas9 KO of *Nprl3 in vitro* resulted in mTOR signaling hyperactivation and mTOR-

dependent abnormalities in cell size and subcellular translocation of mTOR to the lysosomal membrane. Focal *Nprl3* KO using *in utero* electroporation (IUE) caused mTOR-dependent cortical lamination defects and increased seizure susceptibility, both of which were prevented by the mTOR inhibitor rapamycin.

Materials and methods

NPRL3 variants in the Mennonite Community

The Clinic for Special Children (CSC) is located in Lancaster County, Pennsylvania, USA, an area home to a large number of Plain (Amish and Mennonite) families. The CSC also cares for patients of Plain descent from other areas throughout the United States with large Plain settlements. Our Mennonite pedigree was ascertained in a prospective manner to capture the clinical and genetic status of several known *NPRL3* families; through geneologic corroboration and/or cascade testing of relatives to known heterozygotes, the pedigree was expanded into one large pedigree.

NPRL3 heterozygotes (*n=133*; c.349delG, p.Glu117LysFS) were identified from the Mennonite community (2016-2020) through whole exome sequencing, targeted *NPRL3* variant testing, or the Plain Insight Panel, an extended carrier test developed for the Old Order Amish and Mennonite communities. Cascade testing of extended family members was used to identify further potential heterozygotes. Clinical phenotypes were determined through medical interviews (consented over the phone or in writing) with parents of affected children (<18 years old) and adults (≥18 years old); 6 were excluded from the structured medical interview due to a dual genetic diagnosis i.e., *NPRL3* c.349delG heterozygotes who were known to have a second confirmed genetic condition associated with seizures, as the second condition might confound the etiology of the seizure phenotype. For example, an individual who harbored heterozygous variants in *NPRL3* and *KRIT1* was not included in the analysis. Clinical MRI and EEG reports were retrospectively collected and analyzed.

Association analyses were performed with whole exome sequencing data (Regeneron Genetics Center; RGC). Individual vcf files for each *NPRL3* c.349delG heterozygote (n=83) were parsed using FileMaker Pro (FMP) scripts and uploaded into a custom FMP database housing >4000 Amish and Mennonite exomes (SnpEff and ANNOVAR annotations). Exome variants (n=230,656) were filtered based on genotype quality (>98), allele balance (<2), minor allele frequency (>0.05), and a consistency check for Hardy-Weinberg equilibrium.

Exome sequencing

Exome sequencing was performed (at RGC*; 22)* in 1µg of high-quality genomic DNA prepared for exome-captured libraries (NimbleGen VCRome SeqCap 2.1 or IDT XGen targeted capture reagent). Libraries were sequenced (Illumina HiSeq 2500 or the NovaSeq 6000 platforms) achieving coverage of >85% of bases at 20x or greater. Raw sequence reads were mapped and aligned to the GRCh38/hg38 human genome reference assembly using a cloud-based bioinformatics production pipeline that uses BWA-mem for mapping and alignment and GATK HaplotypeCaller for variant and genotype calling. Variants were annotated using an RGC implemented analysis and annotation pipeline that uses Annovar and customized Perl scripts.

CRISPR/Cas9 construct generation and validation

Validated guide RNAs (gRNAs) targeting mouse *Nprl3* were calculated *in silico* using ChopChop software (chopchop.cbu.uib.no). Two gRNAs (*Nprl3* (A) and *Nprl3* (B)) targeting exon 5 of *Nprl3* were used for these experiments (Fig. 2A). A scramble gRNA sequence was used as a transfection and gRNA control. *Nprl3* sequence misalignments generated by CRISPR/Cas9 *Nprl3* editing were confirmed by sequencing (Supplemental Data A-D).

RT-qPCR was used to define changes in *Nprl3* mRNA expression after KO using three biological replicates of each line. Total RNA was extracted from cell pellets of *Nprl3 A* and *B* KO lines, scramble, and WT cells using the RNeasy Mini Kit. RNA was converted to cDNA using a high capacity cDNA reverse transcription kit. RT-qPCR was run using the following primers within *Nprl3 A/B* edited regions: F= AGAAACCTAGTGGCAAGGAATG; R= ATCCTGAAGTGCTAGGATCAGC. Mouse GAPDH was used as an expression control (F= AGGTCGGTGTGAACGGATTTG ; R= TGTAGACCATGTAGTTGAGGTCA). Using SYBR Power Green PCR master and primers described above, a standard dilution was created using WT cDNA at the following concentrations: 1:20, 1:60, 1:180, 1:540, 1:1620. Negative controls used were DNAse free water and diluted random primers. Each sample was loaded into a MicroAmp optical 384-well reaction plate at 1:20 and topped with a MicroAmp adhesive film. Plates was assayed using Viia7 qPCR machine. Analysis was performed as described previously. [22]

Nprl3 KO Cell Lines

Neuro2a cells (N2aC; Sigma-Aldrich) were transfected with CRISPR/Cas9-plasmid using Lipofectamine LTX with Plus reagent (ThermoFisher Scientific) for 48 hours. Transfected N2aC were assayed by flow cytometry (University of Maryland School of Medicine Flow Cytometry Core) sorting based on mCherry (Cas9) fluorescence. mCherry+ sorted cells were re-plated in complete media and grown to confluence.

Soma Diameter

In vitro, cell soma diameter was measured in digital images[23] across the longest dimension of each soma (25 cells in each of 2 biological replicates). To define the mTOR-dependency of cell size changes, cells were incubated for 24 hours with the mTOR inhibitors rapamycin (50 nM, Cell Signaling Technologies) or torin1, a highly selective mTORC1 and mTORC2 kinase inhibitor (50 nM, Tocris) using DMSO as a vehicle control (one-way ANOVA, $p<0.05$).

In electroporated mouse pups (below), soma diameter was measured in GFP labeled neurons in digital images. The longest dimension of the soma was measured in 10 neurons from 5 different animals (50 total) for each experimental group (one-way ANOVA, $p<0.05$).

Lysosomal mTORC1 Activity

Cells were transfected with the CFP/YFP FRET biosensor TORCAR (m**TORC**1 **A**ctivity **R**eporter), cultured for 24 hours in complete DMEM imaging media and imaged on a Zeiss LSM Duo slit-scanning confocal microscope. Images at 20x magnification recording CFP and YFP channel fluorescence were obtained using time-lapse imaging at two-minute intervals for 60 minutes. Following a 10-minute baseline in complete imaging media, distinct experimental media i.e., fresh complete media, AAF imaging media, or complete media with torin1 (50 nM) were added ($n=10$ cells per condition).

The CFP to YFP ratio (C:Y) was calculated for each cell and then averaged (n=10 cells per group; Origin statistical software) within experimental groups, accounting for imaging focal plane fluctuations in living cells and differences in transfection efficiency. Percent change and statistical significance was determined using the average C:Y ratio during a 60-minute baseline in complete media as the comparator for each experimental group (one-way ANOVA, $p<0.05$).

Cell Aggregation

Nprl3 KO, scramble, and WT N2aC were plated at equal density into video dishes for 24-hours. Video dishes were placed into an Olympus VivaView imaging incubator at 37°C with 5% CO_2. Three regions of interest (a 4X magnification field) were selected in each of four video dishes (*Nprl3* A, *Nprl3* B, scramble, WT). Images were taken at 10x every 15 minutes for 48 hours. Quantification of aggregate volume and number was defined in Bitplane using the surface tool. In separate experiments, rapamycin (50nM) or torin1 (50 nM) was added to cell culture media immediately prior to imaging. Time-lapse images were compiled into videos for analysis.

Western Assay

Cells were lysed in RIPA lysis buffer with protease and phosphatase inhibitors. Lysate supernatants were run on a Bolt BT Plus 4-12% gel (Invitrogen) and transferred onto PVDF membranes at 4°C. Membranes were probed overnight at 4°C with antibodies recognizing PS6 or S6 ribosomal protein (mouse monoclonals; 1:500; Cell Signaling). β-actin (1:10,000, rabbit polyclonal; Abcam) was used to ensure equal protein loading. Blots were performed in triplicate using technical replicates for densitometry analysis (Origin software).

Immunocytochemistry (ICC) and Immunohistochemistry (IHC)

Fixed N2aC were probed with primary antibodies: filamentous (F)-actin (1:1000; mouse monoclonal, Abcam), lysosome-associated membrane protein 2, (LAMP2; 1:1000; mouse monoclonal; Thermofisher), mTOR (1:1000; rabbit monoclonal; Abcam), or phospho-ribosomal S6 protein (PS6; Ser240/244; rabbit monoclonal; 1:1000; Cell Signaling). Secondary antibodies (Alexa Fluor488 or Alexa Fluor594; all 1:1000 dilution; Molecular Probes) were incubated with the cells for 2 hours at RT.

Whole brains were post-fixed in 4% PFA overnight (12-hours for P3 pups, 24-hours for adult mice), paraffin embedded, microtome sectioned at 8µm and probed with CTIP2 (1:500; rat monoclonal; Abcam), GFP (1:1000; chicken polyclonal; Abcam), MAP2 (1:100; goat polyclonal; Abcam), PS6 (240/244) or ribosomal S6 protein (mouse monoclonals; 1:2000; Cell Signaling) primary antibodies and then secondary antibodies Alexa488, 647, and 594, respectively

After staining, fluorescence intensity quantification was performed on adult mouse brains to

define PS6 (240/244) levels. A far-red (Alexa 647) secondary antibody was used to probe for PS6 (240/244) due the limited overlap in the fluorescence emission spectrum with Alexa 488 (GFP). Z-stack images were taken on a spinning-disk confocal microscope and reconstructed in 3D using Bitplane software. Images were analyzed in Image J by isolating the soma of an individual neuron and measuring the area and integrated density of the cell as well as the background fluorescence (also measured as integrated density) of each image. Mean, integrated density, and background fluorescence were used to calculate the fluorescence intensity of PS6 (240/244) staining normalized to cell size and non-specific background fluorescence. Quantification of normalized fluorescence intensity data (arbitrary units; AU) was performed in Origin statistical software using ANOVA with a $p<0.05$ deemed significant.

mTOR-lysosome Colocalization Analysis

N2aC lines were plated into chamber slides for 24-hours, then incubated in amino acid free (AAF) or complete media for 60 minutes. Fixed cells probed with mTOR and LAMP2 primary and secondary antibodies (below) were visualized on a spinning disk confocal microscope (Nikon). Fluorescence intensity of mTOR and LAMP2 was measured within a region of interest (ROI; ImageJ[23]) reconstructed into a 3D-fluorescence intensity surface plot. mTOR and LAMP2 fluorescence intensity correlation was determined (Pearson's correlation coefficient, R) with the higher the correlation coefficient, the greater the degree of colocalization between mTOR and LAMP2.

In Utero Electroporation

Timed-pregnant CD1 mouse dams (Charles River) were anesthetized at embryonic day 14 (E14) using isoflurane anesthesia and the uterine horns were surgically exposed as described previously.[24] Separate *Nprl3* (A) and *Nprl3* (B) plasmids (Golden Gate Assembly plus GFP) were micropipetted into the lateral ventricle of 3-7 embryos per dam. Electrode forceps were place on either side of the embryo head and 5 electrical pulses were passed through the embryo to drive the plasmid into neural progenitors lining the telencephalic lateral ventricle. One cohort of dams was treated with a single rapamycin injection (1.0 mg/kg) at 24 hours post-operatively. At P1, pups were examined under a dissecting microscope for GFP fluorescence through the skull. GFP positive pups or littermate controls were selected for IHC analysis and euthanized at P3, or matured to 5 weeks for EEG implantation, seizure threshold testing, and IHC.

The greatest extent of electroporation i.e., GFP fluorescence, was identified and 3 sections of this region from each animal were selected for analysis. Analysis of electroporated and control cortices was performed on 3D reconstructions of Z-stack images taken on a spinning-disk confocal microscope. Regions of electroporation were matched across experimental groups to ensure similar brain regions were being assayed. The number of GFP positive neurons in cortical layers I-VI and the corpus callosum was quantified relative to the total number of GFP positive cells within each section across groups. In addition, soma diameter was measured in layer II neurons in each experimental group.

EEG Recording

EEG electrodes were implanted at five weeks of age and secured onto the skull 3mm behind bregma under isoflurane anesthesia. Continuous EEG recordings (48 hours) were performed using Pinnacle Technology 3 channel EEG system (Lawrence, KS, USA). Sirenia Seizure Pro software (Pinnacle Technology, Lawrence, KS) was used to calculate line length as the sum of the absolute values between neighboring data points over time and total EEG power defined as the total amount of activity across all frequency domains. Electroporated mice from dams with and without rapamycin treatment, or WT mice, were administered the pro-convulsant agent pentylenetetrazol (PTZ) at 55 mg/kg i.p[25] and recorded for 40 minutes to capture the time to first electrographic seizure detected by EEG. Forty minutes after PTZ injection, the experiment was terminated, and animals were euthanized using CO_2 asphyxiation and cervical dislocation. Latency to seizure was assessed manually using EEG recordings.

Statistical Analysis

To determine *NPRL3* variant expression in our patient cohort, surviving variants (n=57,151) were analyzed by chi-square statistic to assess differences in minor allele frequencies within the *NPRL3* c.349delG cohort. The differences in effects of *Nprl3* KO on S6 phosphorylation and cell soma diameter were determined using one-way ANOVA between groups, accepting a range of $p<0.05$ to $p<0.001$ as significant (see Fig. 2 legend). Analysis of 4E-BP1 phosphorylation by FRET, mTOR/lysosome colocalization, and assessment of differential effects of *Nprl3* KO on cell aggregation were assessed by one-way ANOVA. Differences in cortical lamination caused by *Nprl3* KO following in utero electroporation used ANOVA to define significant differences between cell counts in the cortex. Fluorescence intensity quantification of PS6 levels in adult mouse brain was statistically analyzed using

ANOVA with a $p<0.05$ deemed significant. Further statistical details on each experiment can be found in the appropriate results section and figure legends.

Study Approval

This study was approved by the University of Maryland School of Medicine and Lancaster General Hospital Institutional Review Boards and Institutional Animal Care and Use Committees.

Data availability

The data supporting the findings of this study are available from the corresponding author upon reasonable request.

Results

NPRL3 Pedigree

Of 133 *NPRL3* mutation heterozygotes (*NPRL3* c.349delG, p.Glu117LysFS; *n=133*; Fig.1), 48 (36.1%) had a history of seizures while 85 had no seizure history. Of the 48 *NPRL3* individuals with seizures, 42 completed structured medical interviews (6 were excluded from interviews due to a dual genetic diagnosis). Affected individuals displayed markedly heterogeneous epilepsy phenotypes despite sharing the common founder *NPRL3* variant. For example, the median age of seizure onset was 5 years but ranged from one day to 37 years. Clinical seizures subtypes included focal or generalized onset. Six individuals had a history of infantile spasms and 1 reported exclusively febrile seizures. The median peak clinical seizure frequency was 4.5 seizures per day but ranged from 4 per year to >20 per day. The median number of concurrent anti-seizure medications was 2 and ranged from 0 to 4. Within the cohort, the estimated penetrance of seizures was 28% (penetrance may be an underestimate as some patients may develop seizures later in life). Finally, while variants in *DEPDC5*, encoding a protein binding partner (DEPDC5) for NPRL3, have been associated with sudden unexplained death in epilepsy (SUDEP)[7], there were no reported SUDEP cases within our *NPRL3* pedigree.

Available MRI data from 17 and EEG data for 21 *NPRL3* mutation heterozygotes with epilepsy showed highly heterogeneous results (Fig. 1). MRI findings included normal brain structure in 8

individuals and MCD in 9 (FCD, 8 and HME, 1). Nineteen EEGs showed both focal (spikes, sharp waves) and generalized (generalized spike and wave discharges, and/or slowing) abnormalities while two individuals had normal EEGs (these had no MRI available). Interestingly, all cases with normal brain MRI had epileptiform EEG findings i.e., inter-ictal or seizures; 2 cases where MRI was not available, had normal EEG. One individual in the pedigree with a single clinical seizure did not harbor the *NPRL3* c.349delG variant.

Genetic Modifiers of Penetrance

We performed whole exome sequencing (WES) on all *NPRL3* c.349delG heterozygotes to investigate whether any coding sequence variants affected seizure penetrance using a chi-square statistic comparing a seizure-free group (n=37) to those with epilepsy (n=24). Variants passing all filters and demonstrating significant chi-square values (>3.84) are found in Supplemental Table A. Using both the chi-square statistic and the genotype classes, we failed to find a single exome variant that could explain the differences in epilepsy penetrance in our *NPRL3* c.349delG cohort.

mTOR Pathway Activation

Enhanced phosphorylation of ribosomal S6 protein (PS6; Ser240/244) has been reported in resected human *NPRL3* brain tissue [21] and in experimental models of *Nprl3* loss [15,21] as a read-out for mTOR activation. We observed increased PS6 levels in lysates from two distinct *Nprl3* KO N2a cell lines (Figs. 2A and 2B) compared to scramble and WT cells. As expected, PS6 levels were reduced in *Nprl3* KO lines treated with mTOR inhibitors rapamycin (150 nM) or torin1 (100 nM) (Fig. 2B). Next, since the GATOR1 complex inhibits mTOR activity in response to low cellular amino acid levels in non-neural cells i.e., under conditions unfavorable for cell growth, we hypothesized that *Nprl3* KO would abrogate this effect of GATOR1 on mTOR in low amino acid conditions, resulting in persistent mTOR signaling. Indeed, while PS6 levels were reduced in scramble and WT N2aC grown in amino acid free (AAF) media, PS6 levels remained elevated following *Nprl3* KO in AAF media (Fig. 2B). Thus, *Nprl3* KO alters GATOR1 function and is permissive to constitutive mTOR activation even when nutrient conditions are unfavorable for growth. Quantification of Western assays and unedited blots can be found in Supplemental Fig. 1.

Increased Soma Size

Dysmorphic neurons in resected human FCDII tissue samples from epilepsy patients with *NPRL3* variants are larger than control neurons.[15,21] Thus, we hypothesized that *Nprl3* KO would result in mTOR-dependent increases in soma diameter. A 2-fold increase ($p<0.001$) in soma diameter was observed in F-actin labeled *Nprl3* KO cells compared to WT N2a cells (50 cells per group; Fig. 2C,D). Rapamycin (50 nM) or torin1 (50 nM) treatment for 24 hours led to reduction in soma diameter (Fig. 2D) equivalent to WT ($p<0.001$) demonstrating that enhanced cell size following *Nprl3* loss was mTOR-dependent.[14,15]

Altered Subcellular mTOR Localization on the Lysosome

mTORC1 is active as a kinase when tethered to the lysosome. In non-neural cells, GATOR1 prevents translocation of mTORC1 to the lysosomal surface from the cytoplasm when intracellular amino acids are low[12] i.e., conditions unfavorable for cell growth, thereby inhibiting mTOR activity; to date, this has not been studied in neurons. When conditions shift to nutrient deprived, GATOR1 shifts mTORC1 off of the lysosome to the cytoplasm to an inactive conformation.[12] In *Nprl3* KO N2aC (above), PS6 levels were not altered in AAF conditions demonstrating that the effects of *Nprl3* loss on GATOR1 modulation of mTOR signaling are not blocked by nutrient deprivation. Thus, we next investigated the effect of *Nprl3* KO on mTOR subcellular localization under AAF conditions, hypothesizing that *Nprl3* KO would result in persistent co-localization of mTOR on the lysosome even under nutrient deprivation. *Nprl3* KO, scramble control, and wildtype N2aC were incubated in complete or AAF media for 60 minutes, fixed, probed with anti-mTOR and anti-LAMP2 antibodies and imaged on a spinning-disk confocal microscope to define the correlation coefficient between mTOR and LAMP2 fluorescence intensity (Pearson's coefficient, R; Fig.3A). In complete media (nutrient replete conditions), there was a high correlation between mTOR and LAMP2 expression, with mTOR highly co-localized to the lysosome (Fig. 3A, B; $R \geq 0.9$ for each group; n=10 per group). In contrast, mTOR dissociates from the lysosomal surface in WT and scramble N2aC in AAF media evidenced by greater cytoplasmic mTOR localization ($p<0.05$; R-values of 0.78 and 0.77, respectively, Fig. 3B). In *Nprl3* KO cells, mTOR and LAMP2 expression remained co-localized on the lysosome (R = 0.89 and 0.92 for *Nprl3 (A)* and *Nprl3 (B)*, respectively) when incubated AAF media. Thus, *Nprl3* KO allows mTOR to remain inappropriately localized to the lysosomal membrane in an activated conformation (evidenced by persistent phosphorylation of S6 protein, above) even under AAF conditions, demonstrating that *Nprl3* KO decouples mTOR subcellular localization and activation from modulation by metabolic state via GATOR1.[10]

Activation of mTOR in live neurons at the lysosomal membrane

Phosphorylation of the mTOR substrate eukaryotic translation initiation factor 4E (eIF4E)-binding protein-1 (P4E-BP1; Thr36/47) serves as a measure of mTOR activation (akin to S6 protein, above). We used the CFP/YFP FRET biosensor TORCAR which targets the lysosomal membrane via LAMP1 (like LAMP2, above, a lysosomal membrane protein), coupled to 4E-BP1. [26,27] The ratio of CFP to YFP (C:Y) fluorescence provides a bioassay of dynamic changes in 4E-BP1 phosphorylation (increases or decreases) at the lysosomal surface in living cells. As 4E-BP1 phosphorylation is unaffected by rapamycin,[28,29] TORCAR-transfected *Nprl3* KO, scramble, and WT N2aC were treated with torin1 in complete media for one hour (Supplemental Fig. 3;). The effects of torin1 are rapid, with progressive reduction in C:Y ratio, reflecting reduced P4E-BP1 levels, by 7.5% (*Nprl3* (A)) and 5.7% (*Nprl3* (B) ($p<0.001$; Fig. 3F,G) within 50 minutes (Supplemental Fig. 4). We next assayed the effects of nutrient deprivation. While scramble and WT N2aC incubated in AAF media exhibited an appropriate reduction in C:Y ratio (WT, 9.4% and scramble, 5.7%; $p<0.001$; Fig. 3D,F), *Nprl3* KO N2aC lines showed persistent and inappropriate 4E-BP1 phosphorylation (Fig. 3D,F), unaltered by AAF exposure; this effect is similar to S6 phosphorylation data above.

Together, the P4E-BP1 and PS6 data show mechanistically that *Nprl3* KO abrogates the effects of GATOR1 on mTOR subcellular localization and activation in response to nutrient deprivation, that nutrient deprivation cannot override the effects of *Nprl3* KO on mTOR activation, and importantly, that *Nprl3* KO drives mTOR activation over a range of metabolic conditions in neurons, decoupling mTOR from metabolic signaling.

Cellular Aggregation

Human FCDII specimens exhibit cytomegalic dysmorphic neurons that may be observed occurring in close physical apposition (aggregates).[30] Interestingly, *Tsc1* KO astrocytes grow in clumps or aggregates *in vitro,*[31] and a *Tsc2* KO mouse strain shows heterotopic cell clumps ("ring heterotopias") in the hippocampus.[35] Since human *NPRL3* variants are linked to FCDII histopathology, we hypothesized that *Nprl3* KO would cause abnormal cellular aggregation *in vitro.* N2aC typically grow in a monolayer with limited cell stacking *in vitro*. Thus, abnormal cellular aggregates were operationally defined using z-stack confocal imaging of closely apposed cells (no space between cell membranes) achieving an aggregate volume of >200 mm^3. We first examined whether aggregates formed in live cells visualized by

time-lapse bright-field imaging. *Nprl3* KO N2aC formed large aggregates ("clumps", mean volume 600mm^3; Fig.4) that progressively grew by accumulating cells from the surrounding environment over the 48-hour imaging epoch. Dynamic video analysis revealed cells readily adhering to, but not detaching from, aggregates (Supplemental Video 1). The formation of cell aggregates was prevented with rapamycin (50 nM) or torin1 (50 nM; Supplemental Videos 2 and 3) treatment for 48-hours and during treatment, cells were observed moving freely within the recorded region rather than sticking to growing aggregates. In contrast, cell aggregates were not noted in control lines (Supplemental Video 1; Fig. 4); small accumulations (<100mm^3) of cells is typical of WT and scramble N2a cells.

We next examined total aggregate volume, aggregate number, and cell number within aggregates in *Nprl3* KO cells using spinning-disk confocal microscopy in 3D (Fig.4). Aggregate volume (n=10 per group; *inset* in Fig. 4B) in *Nprl3* KO N2aC lines exceeded 600mm^3 compared to scramble and WT lines (Fig. 4A). The total number of cell aggregates in *Nprl3* KO N2aC lines (>60 aggregates per region) was dramatically increased compared to control N2aC lines (Fig. 4B). The total number of cells in each aggregate was quantified by counting the nuclei in each aggregate (n=10 aggregates per group) and revealed statistically significant increases in cell number in *Nprl3* KO N2aC lines versus scramble and WT N2aC controls (Fig. 4D). Increases in aggregate number, volume, and increases in cell number per aggregate in *Nprl3* KO cells were prevented with rapamycin (50 nM) or torin1 (50 nM) demonstrating that aberrant cell aggregation following *Nprl3* KO was mTOR-dependent (Fig 4C-E). Of note, enhanced cell proliferation (determined via EdU assay) was not observed (Supplemental Fig. 2). Thus, mTOR-dependent cell aggregate formation did not result from enhanced cell proliferation.

Nprl3 and Cerebral Cortex Structure

To model the effect of *NPRL3* gene inactivation in the developing human brain,[34] we used *in utero* electroporation (IUE) to transfect *Nprl3* (A) and (B) gRNAs and Cas9/GFP plasmids into neuroglial progenitor cells in the telencephalic ventricular zone on embryonic day (E14). Pups were euthanized on P3 and brain sections were probed with anti-GFP antibodies to visualize cells with *Nprl3* KO. Anti-CTIP2 antibody co-labeling was used to define layer IV-VI neurons in *Nprl3* KO and scramble transfected neurons.

All GFP-labeled neurons were observed in layer II/III in scramble gRNA electroporated pups consistent with cell fate destination to layer II/III for progenitor cells born at E14. In contrast, numerous GFP-labeled neurons were observed in deeper cortical layers IV-VI and in the subcortical white matter in

Nprl3 KO P3 mouse pups (n=5; Fig. 5A). Deep layer GFP-labeled neurons in *Nprl3* KO pups did not co-express CTIP2. We submit that since the timepoint at which we electroporated each pup (E14) yields neurons with a layer II/III identity, the lack of CTIP2 expression in heterotopic neurons suggests improper positioning of neurons in the white matter destined for layer II/III. GFP-labeled neurons in *Nprl3* KO pups were larger than in scramble transfected pups ($p<0.0001$; Fig. 5A, C) commensurate with observations following *Nprl3* KO *in vitro* (Fig. 2).

We next assayed whether mTOR inhibition during corticogenesis would rescue the effects of *Nprl3* KO on cortical lamination while avoiding the need for ongoing treatment. Pregnant dams were treated with rapamycin (1.0 mg/kg; single dose IP) 24 hours after IUE surgery (approximately E15). The half-life of rapamycin is approximately 60 hours so a single dose at E15 will affect mTOR activation in neural progenitors until late stages of corticogenesis i.e., E18. When assayed at P3, the laminar defects observed in *Nprl3* KO pup brain sections were rescued by rapamycin with the preponderance of GFP-labeled cells observed in the appropriate layer II/III position (Fig. 5B, C). Further histopathological examination of *Nprl3* KO pups revealed normalization of cell size in all *Nprl3* KO GFP-labeled cells to WT size.

Excitability and Seizure Threshold

In the 5 weeks prior to EEG electrode implantation, no behavioral seizures were observed during twice daily observation of electroporated mice. At 5 weeks post-electroporation, dural electrodes were implanted over the electroporated cortical regions. EEGs were recorded for 48 hours and no spontaneous seizures were observed in *Nprl3* KO or scramble control mice (n= 6 per group). To define subtle electrographic changes that may indicate seizure propensity, we extracted line length as a measure of signal amplitudes, and total EEG power data, a measure of frequency band activity, from continuous EEG recordings for left and right hemispheres of KO and WT animals. In the electroporated cortices of *Nprl3* KO mice, higher signal amplitudes i.e., increased EEG activity were observed compared to non-electroporated hemisphere and to WT mice (Fig. 5F). Increased line length (Fig. 5F; *arrow*) observed in the electroporated cortex did not correspond to increased line length in the contralateral cortex and therefore increased cortical activity in the electroporated cortex was independent of activity in the contralateral cortex. In contrast, WT mice exhibit similar overall line length, and thus similar levels of cortical activity, in both left and right hemispheres (Fig. 5F). These data were further quantified by total power

data that revealed an increase in EEG power in the electroporated hemisphere of *Nprl3* KO mice compared to the non-electroporated hemisphere and to WT mice (Fig. 5G). Rapamycin treatment after *Nprl3* KO rescued increased line length and total power seen in *Nprl3* KO hemispheres (Fig. 5F, G). Together, these data point toward an mTOR-dependent increase in cortical activity in *Nprl3* KO mice compared to control.

Seizure threshold was assayed in mice injected with pentylenetetrazol (PTZ; 55 mg/kg).[33] *Nprl3* KO mice displayed a significant decrease in seizure latency from time of PTZ injection to onset of first electrographic seizure (77.2 sec; SEM=11 sec) compared to WT mice (168 sec; SEM=34 sec; $p<0.05$; Fig. 5 H,I). Rapamycin treatment rescued seizure threshold as *Nprl3* KO pups from dams treated with rapamycin had a seizure threshold (latency) similar to WT mice (178 sec; SEM=52 sec; Figure 5 H, I). Histological examination of implanted *Nprl3* KO cortices at 5 weeks post-IUE (n= 6) revealed that lamination defects, (GFP-labeled neurons in cortical layers IV-VI), persisted similar to P3 pups (Fig. 5E). Thus, mTOR inhibition rescued seizure threshold independent of cortical laminar abnormalities. Histological sections from 5-week old *Nprl3* KO and WT littermate mice were also assayed for PS6 (240/244) levels using fluorescence intensity analysis (n=4 per group). We observed a statistically significant increase in PS6(240/244) in GFP+ (KO) neurons while neurons within the electroporated region but not GFP+ has similar levels of PS6 fluorescence as WT littermate controls (Fig 6; $p<0.001$; n= 30 neurons per group). Total S6 levels were observed to be similar between GFP+ and adjacent GFP- neurons irrespective of PS6 (240/244) levels (Supplemental Fig. 5).

Discussion

We present the largest and oldest assembled founder *NPRL3* pedigree reported to date originating within an Old Order Mennonite couple in the 1720's. As in non-Mennonite *NPRL3* individuals,[34] there was a wide spectrum of clinical seizure phenotypes, EEG features, and MRI findings, despite a common genotype in our cohort. As a strategy to understand how *NPRL3* loss causes these phenotypes, we show that *Nprl3* KO induces mTOR-dependent increases in soma diameter both *in vitro* and *in vivo*. We demonstrate for the first time in neurons the effects of *Nprl3* KO on GATOR1 modulation of mTOR in low nutrient conditions and show a mechanism by which mTOR remains activated following *Nprl3* KO i.e., persistent localization of mTOR to the lysosome even under nutrient deprived conditions. A unique feature of *Nprl3* loss *in vitro* is enhanced cellular aggregation, prevented with mTOR inhibition.

Focal *Nprl3* KO in fetal mouse brain *in vivo* causes results in heterotopic neurons in the white matter and reduced PTZ-induced seizure thresholds, both phenotypes that were rapamycin sensitive. Importantly, our results are bolstered by findings in mice lacking *Depdc5*[16,17] suggesting a mechanistic association between DEPDC5 and NPRL3, known protein binding partners within GATOR1.

The penetrance of epilepsy in our cohort was 28%. In *NPRL3* patients with epilepsy, MRI findings revealed a spectrum ranging from no visible abnormalities to HME, ours being only the second reported case of HME associated with *NPRL3.*[9] Interestingly, the most severe seizure phenotypes were not always observed in patients with the most abnormal MRIs and in some individuals with seizures, brain MRI was normal suggesting either microscopic structural changes in the cortex or potentially, autonomous effects of NPRL3 loss on network excitability.

As a strategy to understand phenotypic variability, we reasoned that our large pedigree with common Mennonite haplotype background provided a unique opportunity to assess the effects of a modifier gene on seizure penetrance as, to date, no study has assessed genetic modifiers as a cause for clinical heterogeneity in MCD and epilepsy in mTORopathies. We readily acknowledge that whole genome sequencing (WGS) would give the most comprehensive picture of gene modifiers for seizure phenotype within the genetic context of a founder *NPRL3* mutation. Virtually all patients evaluated at the Clinic for Special Children undergo WES, so we used this remarkable resource to seek exonic variants that might alter seizure phenotype. Our deep analysis did not yield single gene exon variants that might account for differences in seizure phenotype across this *NPRL3* c.349delG cohort. So, while we cannot definitively say that there were no gene modifiers detected *genome-wide*, we can with confidence say that no modifiers were detected within wholly sequenced exomes, a finding that has not been previously reported in mTORopathies. This approach enabled us to exclude additional pathogenic variants in genes associated with seizure phenotypes within the compared cohorts and exclude any single gene variants within the exome, a necessary first step given the nature of enriched alleles within founder populations. Future whole genomic and epigenomic studies will be useful approaches to identify genetic modifiers with smaller or additive effects to seizure phenotype expression. Of course, we acknowledge that multiple polygenic modifiers may act independently in each individual or sibship or that our sample size is too small to detect modifiers. However, our data suggest an alternate mechanism through which heterozygous *NPRL3* genotypes result in partially penetrant and clinically heterogeneous phenotypes.[4] Finally, in contrast to *DEPDC5* variants, the Mennonite *NPRL3* variant does not appear to be associated with SUDEP as there were no cases of possible or confirmed SUDEP within

this large cohort.[7] Indeed, while sudden death was a phenotype observed in *Depdc5*-SynCre mice[18] early death was not a feature in our mice after focal *Nprl3* KO.

We show that *Nprl3 KO* resulted in persistent and inappropriate mTOR localization on the lysosomal membrane with ongoing signaling as evidenced by 4E-BP1 phosphorylation, even under nutrient deprived conditions. To date, no study has investigated lysosomal mTOR co-localization in living neurons or effects of a specific mTOR pathway gene on subcellular mTORC1 localization. Our data demonstrate that *NPRL3* variants augment mTOR hyperactivation by allowing inappropriate and constitutive localization of mTORC1 to the lysosomal membrane in an active signaling conformation, even when unfavorable metabolic cellular demands require mTOR inhibition.[10,15] The implications of these data are that loss of NPRL3 (and potentially NPRL2 and DEPDC5) are fully permissive to constitutive mTOR signaling across a wide range of neuronal metabolic states.

Excessive cell aggregation is observed in models of tuberous sclerosis complex (TSC) including aggregation of *Tsc1* KO astrocytes *in vitro* and formation of ring heterotopias in *Tsc2* KO neurons *in vivo*.[31,35] We show that *Nprl3* KO led to excessive and mTOR-dependent cellular aggregation *in vitro* prevented with rapamycin. In TSC, changes in cell adhesion molecule (CAM) expression have been observed in human specimens [36-38] that may explain increased cellular aggregation e.g., expression of CAMs may lead to enhanced adhesiveness of cells. Changes in cell adhesion could compromise neuronal motility during cortical development leading to altered cortical laminar organization.

In mice, focal *in utero Nprl3* KO led to neuronal enlargement and heterotopic neurons in white matter modeling several features of human *NPRL3*- and *DEPDC5*-associated FCD[39] and mouse *Depdc5* KO *in vivo.*[16,17] Increased cell size (*in vitro* and *in vivo*) and laminar malpositioning were rescued with mTOR inhibitors. NPRL3 and DEPDC5 are functional binding partners within GATOR1 and may lead to similar, though not identical, histopathological phenotypes by mTOR-dependent mechanisms. While *Nprl3* KO did not result in spontaneous electrographic or behavioral seizures seen in a conditional mouse *Depdc5* KO strain or following *Depdc5* KO in rat, [16,17] focal *Nprl3* KO (via IUE) and strain differences (rat versus mouse) could account for these disparities. However, we observed a decrease in seizure threshold in *Nprl3* KO mice suggesting that *Nprl3* KO led to a hyperexcitable network that was rescued by rapamycin.

Our data demonstrate new links between *Nprl3* KO and mTOR pathway hyperactivation, abnormal neuronal morphology, altered metabolic control of mTOR, disorganized cerebral cortical

lamination, and enhanced seizure susceptibility that provides insights into the clinical phenotypic variability observed in *NPRL3* individuals. The absence of a detected modifier gene variant in this cohort argues that clinical phenotype is largely dictated by *NPRL3* loss. Importantly, we show that mTOR inhibition can rescue effects on cell and brain structure and network excitability caused by *Nprl3* KO and thus, these findings provide a pre-clinical platform for future studies examining the efficacy of mTOR inhibitors in patients with GATOR1 gene variants.

Acknowledgements

NPRL3 patients and their families; Dr. Joseph Mauban, Manager of the University of Maryland School of Medicine Confocal Microscopy core, for his assistance with both live-cell slit-scanning and spinning disk confocal microscopy; Dr. Xiaoxuan Fan, Director of the Flow Cytometry Shared Service at the University of Maryland for his assistance in establishing CRISPR cell lines; Ryan Richardson at the University of Maryland School of medicine for assistance in generating PX330 CRISPR plasmids; Philip H. Iffland, DDS for assistance with improving the EEG implantation technique. *Nprl3* sequence misalignments generated by CRISPR/Cas9 *Nprl3* editing were confirmed by Massachusetts General Hospital Center for Computational and Integrative Biology DNA Core for whole amplicon next-generation sequencing. TORCAR, courtesy J. Zhang, John Hopkins University and Addgene plasmid # 64929; http://n2t.net/addgene:64929; RRID:Addgene_64929.

Funding

This work was supported by NINDS R01NS099452 and R01NS094596 (PBC).

Competing interests

The authors report no competing interests.

Supplementary material

Supplementary material is available at *Brain* online.

References

1. Crino PB. mTOR signaling in epilepsy: insights from malformations of cortical development. *Cold Spring Harb Perspect Med*. 4/2015 2015;5(4)Not in File. doi:5/4/a022442 [pii];10.1101/cshperspect.a022442 [doi]
2. Osborne LR. Caveat mTOR: aberrant signaling disrupts corticogenesis. *J Clin Invest*. May 2010;120(5):1392-5. doi:10.1172/JCI43030
3. Iffland PH, Crino PB. Focal Cortical Dysplasia: Gene Mutations, Cell Signaling, and Therapeutic Implications. *Annu Rev Pathol*. 1/24/2017 2017;12:547-571. Not in File. doi:10.1146/annurev-pathol-052016-100138 [doi]
4. Baulac S. mTOR signaling pathway genes in focal epilepsies. *Prog Brain Res*. 2016 2016;226:61-79. Not in File. doi:S0079-6123(16)30039-5 [pii];10.1016/bs.pbr.2016.04.013 [doi]
5. Baldassari S, Licchetta L, Tinuper P, Bisulli F, Pippucci T. GATOR1 complex: the common genetic actor in focal epilepsies. *J Med Genet*. 8/2016 2016;53(8):503-510. Not in File. doi:jmedgenet-2016-103883 [pii];10.1136/jmedgenet-2016-103883 [doi]
6. Weckhuysen S, Marsan E, Lambrecq V, *et al*. Involvement of GATOR complex genes in familial focal epilepsies and focal cortical dysplasia. *Epilepsia*. 6/2016 2016;57(6):994-1003. Not in File. doi:10.1111/epi.13391 [doi]
7. Baldassari S, Picard F, Verbeek NE, *et al*. The landscape of epilepsy-related GATOR1 variants. *Genet Med*. Feb 2019;21(2):398-408. doi:10.1038/s41436-018-0060-2
8. D'Gama AM, Woodworth MB, Hossain AA, *et al*. Somatic Mutations Activating the mTOR Pathway in Dorsal Telencephalic Progenitors Cause a Continuum of Cortical Dysplasias. *Cell Rep*. Dec 26 2017;21(13):3754-3766. doi:10.1016/j.celrep.2017.11.106
9. Canavati C, Klein KM, Afawi Z, *et al*. Inclusion of hemimegalencephaly into the phenotypic spectrum of NPRL3 pathogenic variants in familial focal epilepsy with variable foci. *Epilepsia*. Jun 2019;60(6):e67-e73. doi:10.1111/epi.15665
10. Bar-Peled L, Chantranupong L, Cherniack AD, *et al*. A Tumor suppressor complex with GAP activity for the Rag GTPases that signal amino acid sufficiency to mTORC1. *Science*. 5/31/2013 2013;340(6136):1100-1106. Not in File. doi:340/6136/1100 [pii];10.1126/science.1232044 [doi]
11. Sancak Y, Sabatini DM. Rag proteins regulate amino-acid-induced mTORC1 signalling. *Biochem Soc Trans*. Feb 2009;37(Pt 1):289-90. doi:10.1042/BST0370289

12. Wolfson RL, Sabatini DM. The Dawn of the Age of Amino Acid Sensors for the mTORC1 Pathway. *Cell Metab*. Aug 1 2017;26(2):301-309. doi:10.1016/j.cmet.2017.07.001

13. Dibbens LM, de Vries B, Donatello S, *et al*. Mutations in DEPDC5 cause familial focal epilepsy with variable foci. *Nature genetics*. May 2013;45(5):546-51. doi:10.1038/ng.2599

14. Yuskaitis CJ, Rossitto LA, Gurnani S, Bainbridge E, Poduri A, Sahin M. Chronic mTORC1 inhibition rescues behavioral and biochemical deficits resulting from neuronal Depdc5 loss in mice. *Hum Mol Genet*. Sep 1 2019;28(17):2952-2964. doi:10.1093/hmg/ddz123

15. Iffland PH, 2nd, Baybis M, Barnes AE, Leventer RJ, Lockhart PJ, Crino PB. DEPDC5 and NPRL3 modulate cell size, filopodial outgrowth, and localization of mTOR in neural progenitor cells and neurons. *Neurobiol Dis*. Jun 2018;114:184-193. doi:10.1016/j.nbd.2018.02.013

16. Hu S, Knowlton RC, Watson BO, *et al*. Somatic Depdc5 deletion recapitulates electroclinical features of human focal cortical dysplasia type IIA. *Annals of neurology*. Jul 2018;84(1):140-146. doi:10.1002/ana.25272

17. Ribierre T, Deleuze C, Bacq A, *et al*. Second-hit mosaic mutation in mTORC1 repressor DEPDC5 causes focal cortical dysplasia-associated epilepsy. *J Clin Invest*. Jun 1 2018;128(6):2452-2458. doi:10.1172/JCI99384

18. Yuskaitis CJ, Jones BM, Wolfson RL, *et al*. A mouse model of DEPDC5-related epilepsy: Neuronal loss of Depdc5 causes dysplastic and ectopic neurons, increased mTOR signaling, and seizure susceptibility. *Neurobiol Dis*. Mar 2018;111:91-101. doi:10.1016/j.nbd.2017.12.010

19. de Calbiac H, Dabacan A, Marsan E, *et al*. Depdc5 knockdown causes mTOR-dependent motor hyperactivity in zebrafish. *Annals of clinical and translational neurology*. May 2018;5(5):510-523. doi:10.1002/acn3.542

20. Marsan E, Ishida S, Schramm A, *et al*. Depdc5 knockout rat: A novel model of mTORopathy. *Neurobiol Dis*. 5/2016 2016;89:180-189. Not in File. doi:S0969-9961(16)30031-6 [pii];10.1016/j.nbd.2016.02.010 [doi]

21. Ricos MG, Hodgson BL, Pippucci T, *et al*. Mutations in the mTOR pathway regulators NPRL2 and NPRL3 cause focal epilepsy. *Ann Neurol*. 10/27/2015 2015;Not in File. doi:10.1002/ana.24547 [doi]

22. Nugent BM, Wright CL, Shetty AC, *et al*. Brain feminization requires active repression of masculinization via DNA methylation. *Nat Neurosci*. May 2015;18(5):690-7. doi:10.1038/nn.3988

23. Schneider CA, Rasband WS, Eliceiri KW. NIH Image to ImageJ: 25 years of image analysis. *Nat Methods*. Jul 2012;9(7):671-5.

24. Parker WE, Orlova KA, Parker WH, *et al*. Rapamycin prevents seizures after depletion of STRADA in a rare neurodevelopmental disorder. *Sci Transl Med*. 4/24/2013 2013;5(182):182ra53. Not in File. doi:5/182/182ra53 [pii];10.1126/scitranslmed.3005271 [doi]

25. Giardina WJ, Gasior M. Acute seizure tests in epilepsy research: electroshock- and chemical-induced convulsions in the mouse. *Curr Protoc Pharmacol*. Jun 2009;Chapter 5:Unit 5 22. doi:10.1002/0471141755.ph0522s45

26. Zhou X, Clister TL, Lowry PR, Seldin MM, Wong GW, Zhang J. Dynamic Visualization of mTORC1 Activity in Living Cells. *Cell Rep*. Mar 17 2015;10(10):1767-1777. doi:10.1016/j.celrep.2015.02.031

27. Zhou X, Li S, Zhang J. Tracking the Activity of mTORC1 in Living Cells Using Genetically Encoded FRET-based Biosensor TORCAR. *Curr Protoc Chem Biol*. Dec 7 2016;8(4):225-233. doi:10.1002/cpch.11

28. Livingstone M, Bidinosti M. Rapamycin-insensitive mTORC1 activity controls eIF4E:4E-BP1 binding. *F1000Res*. 2012;1:4. doi:10.12688/f1000research.1-4.v1

29. Choo AY, Yoon SO, Kim SG, Roux PP, Blenis J. Rapamycin differentially inhibits S6Ks and 4E-BP1 to mediate cell-type-specific repression of mRNA translation. *Proceedings of the National Academy of Sciences of the United States of America*. Nov 11 2008;105(45):17414-9. doi:10.1073/pnas.0809136105

30. Urbach H, Scheffler B, Heinrichsmeier T, *et al*. Focal cortical dysplasia of Taylor's balloon cell type: a clinicopathological entity with characteristic neuroimaging and histopathological features, and favorable postsurgical outcome. *Epilepsia*. Jan 2002;43(1):33-40. doi:10.1046/j.1528-1157.2002.38201.x

31. Uhlmann EJ, Wong M, Baldwin RL, *et al*. Astrocyte-specific TSC1 conditional knockout mice exhibit abnormal neuronal organization and seizures. *Annals of neurology*. Sep 2002;52(3):285-96. doi:10.1002/ana.10283

32. Blumcke I, Aronica E, Miyata H, *et al*. International recommendation for a comprehensive neuropathologic workup of epilepsy surgery brain tissue: A consensus Task Force report from the ILAE Commission on Diagnostic Methods. *Epilepsia*. 3/2016 2016;57(3):348-358. Not in File. doi:10.1111/epi.13319 [doi]

33. Claycomb RJ, Hewett SJ, Hewett JA. Prophylactic, prandial rofecoxib treatment lacks efficacy against acute PTZ-induced seizure generation and kindling acquisition. *Epilepsia*. Feb 2011;52(2):273-83. doi:10.1111/j.1528-1167.2010.02889.x

34. Sim JC, Scerri T, Fanjul-Fernandez M, *et al*. Familial cortical dysplasia caused by mutation in the mammalian target of rapamycin regulator NPRL3. *Ann Neurol*. 1/2016 2016;79(1):132-137. Not in File. doi:10.1002/ana.24502 [doi]

35. Way SW, McKenna J, 3rd, Mietzsch U, Reith RM, Wu HC, Gambello MJ. Loss of Tsc2 in radial glia models the brain pathology of tuberous sclerosis complex in the mouse. *Hum Mol Genet*. Apr 1 2009;18(7):1252-65. doi:10.1093/hmg/ddp025

36. Boer K, Crino PB, Gorter JA, *et al*. Gene expression analysis of tuberous sclerosis complex cortical tubers reveals increased expression of adhesion and inflammatory factors. *Brain Pathol*. Jul 2010;20(4):704-19. doi:10.1111/j.1750-3639.2009.00341.x

37. Maldonado M, Baybis M, Newman D, *et al*. Expression of ICAM-1, TNF-alpha, NF kappa B, and MAP kinase in tubers of the tuberous sclerosis complex. *Neurobiol Dis*. 11/2003 2003;14(2):279-290. Not in File. doi:S096999610300127X [pii]

38. Arai Y, Takashima S, Becker LE. CD44 expression in tuberous sclerosis. *Pathobiology*. Mar-Apr 2000;68(2):87-92. doi:10.1159/000028118

39. Iffland PH, 2nd, Carson V, Bordey A, Crino PB. GATORopathies: The role of amino acid regulatory gene mutations in epilepsy and cortical malformations. *Epilepsia*. Nov 2019;60(11):2163-2173. doi:10.1111/epi.16370

Figure legends

Figure 1: Old Order Mennonite pedigree with *NPRL3* founder mutation. (A) Probands (n=133) heterozygous for the *NPRL3* c.349delG, p.Glu117LysFS variant. All patients were connected through a twelve-generation pedigree to a founder mutation originating in an Old Order Mennonite couple from Pennsylvania born in 1727 and 1728. Heterozygous individuals are denoted with a cross-mark, while individuals in which the variant was not detected are denoted with a (-) below their symbol. Patients with seizures are denoted in orange. A number below a patient symbol corresponds to the subject number listed in (C) for EEG and MRI results. Of note, only one patient who did not have the *NPRL3* variant reported seizures. *Number inside of diamond represents condensed sibling numbers to conserve pedigree space.* (B) MRI and PET/MRI images for subjects 10, 1, 4, and 12. Subject 10 at age 3 days, T2-weighted image showing left HME with associated cortical thickening (arrow). Subject 1 at age 7 weeks, T2-weighted image showing large left hemispheric cortical dysplasia involving the parietal, temporal, and occipital lobes (arrow). Subject 4 at age 1 year 7 months, T2-weighted image showing focal cortical dysplasia in the right frontal lobe (arrow). Subject 12 at age 7 years 11 months, PET/MRI showing large area of hypometabolism in the left posterior temporal cortex in a patient without obvious focal cortical dysplasia on previous imaging (arrow). (C) MRI and EEG data (see text).

Figure 2: *Nprl3* KO results in mTOR-dependent increases in S6 phosphorylation and soma diameter. (A), *Nprl3* region targeted by *in silico* generated gRNAs targeting exon 5 of the mouse *Nprl3* gene. Vertical black bars represent exons with the thickness of each bar denoting relative size. Exon 5 PCR products assayed by whole amplicon next-generation sequencing showed sequence misalignments in both KO lines (Supplemental Data A-D). Bar graph shows RT-qPCR analysis revealing a decrease in *Nprl3* mRNA levels in KO lines. (B), upper panel, increase in PS6 (240/244) in *Nprl3* KO N2aC in complete media that is reversed with rapamycin (150 nM, 60 min) or torin1 (100 nM; 60 min). Sustained levels of PS6 (240/244) were observed in *Nprl3* KO N2aC after incubation in AAF media vs. scramble and WT cells (AAF media, 60 min). Unedited Western blots and densitometry data for Western assays can be found in Supplemental Fig. 1. (C), Representative images of each cell line are shown showing soma enlargement in Nprl3 KO cells. (D), After *Nprl3* KO, a statistically significant increase in soma diameter was observed in *Nprl3* KO N2aC lines vs. WT and scramble controls (n= 25 cells from each of two biological replicates (50 total cells per group); one-way ANOVA, $p<0.001$). Rapamycin (50 nM, 48hrs) or torin1 (50 nM, 48 hrs) but not vehicle (DMSO), resulted in a statistically significant decrease in soma diameter in *Nprl3* KO N2aC; cell size was reduced by rapamycin and torin1 in control WT and scramble N2a cells as well. In (D),

each box represents the S.E. with a mean line shown, box whiskers represent the 5-95% confidence intervals, diamonds represent individual data points. ***= p<0.001 vs. scram WT and torin1 or rapa, **=p<0.01, *=p<0.05 vs torin1 and rapa, WT= wildtype, WT(U)= untreated wildtype lysate, Scram= scramble, F-actin=filamentous actin, KO= untreated KO, NP3=*Nprl3,* β-actin=beta actin. Calibration mark in (C) = 25 μM

Figure 3: *Nprl3* KO alters mTOR subcellular localization on the lysosome and 4E-BP1 phosphorylation in living cells. (A), Colocalization regions of interest (ROIs; representative ROI are show as insets in A) between mTOR and LAMP2 are orange/yellow in 3D intensity plots and ROIs where mTOR and LAMP2 are not colocalized appear as distinct red and green areas. mTOR and LAMP2 are highly colocalized in control N2a cells in complete media. (B), Graphic depiction of average correlation coefficients determined in (A). Comparing CMP and AAF media, WT and scramble cell lines display a statistically significant decrease (p<0.05) in colocalization between mTOR and the lysosomal membrane (LAMP2) whereas no change in colocalization was observed in *Nprl3* KO cells incubated in AAF media. Boxes represent results from one-way ANOVA, with mean and S.E., whiskers are 5-95% confidence intervals. In (C-G), TORCAR transfected cells, FRET-based C:Y ratio representing 4E-BP1 phosphorylation quantified in *Nprl3* KO, scramble control, and WT N2aC lines. Cells were incubated in AAF media or complete media containing torin1 for 50 minutes. Measurements were taken at two-minute intervals. Statistical significance was calculated in comparison to complete media baseline recordings in (C). Decreases in C:Y (4E-BP1 phosphorylation) were observed in WT (-9.4%) and scramble (-5.7%) N2aC after incubation in AAF media (p <0.01) but no change in C:Y was observed in *Nprl3* A/B KO lines (D,F). mTOR inhibition with torin1 resulted in a significant decrease in C:Y in all experimental groups (E,G; p<0.01) and, unlike AAF media, torin1 treatment of *Nprl3 A/B* KO lines resulted in 7.4% and 5.7% reductions in C:Y, respectively (p<0.01; G). *=p<0.05, **= p<0.01, WT= wildtype, scram= scramble, NP3 (A)=*Nprl3* (A), NP3(B)=*Nprl3* (B), AAF=amino acid free media, CMP=complete media, Calibration mark in (A) = 25 μM.

Figure 4: *Nprl3* KO results in mTOR-dependent cellular aggregation *in vitro.* (A), Representative confocal micrographs reveal large cellular aggregates in *Nprl3* KO lines but not control N2aC lines (time-lapse growth of aggregates visualized in Supp. Video 1). Representative micrographs in (B) show high magnification image of a cellular aggregate in an *Nprl3* KO N2aC line compared to WT N2aC. The volume of each aggregate (n=5 aggregates per group) in *Nprl3* KO N2aC lines is greater than in WT or scramble control N2aC (C; inset in B shows digital surface created to measure aggregate volume; p<0.05). *Nprl3* KO N2aC have significantly increased total aggregate counts (D; p<0.01). *Nprl3* KO

aggregates have a greater cell number than control N2aC as measured by DAPI fluorescence (E; p<0.05). Increases in aggregate number, volume, and cell number were prevented with rapamycin (50 nM; 48 hr.) or torin1 (50 nM; 48 hr.) treatment (C-E; see time-lapse imaging Supp. videos 2-3). **=p<0.01, *=p<0.05, scram=scramble, WT=wildtype, complete=complete physiological media; rapa=rapamycin. Calibration mark in (A) = 500 µm. Calibration mark in (B) = 100 µm.

Figure 5: Focal *Nprl3* KO *in vivo r*esults in lamination defects, increased soma diameter, increased cortical excitability, and reduced seizure threshold. (A,B), GFP+ cells observed in the sub-cortical white matter (bottom arrow) and in layers IV-VI in *Nprl3* KO cortex at P3. In contrast, all GFP+ cells in scramble control specimens (n=5 per groups; p<0.001) were observed in the birthdate appropriate layer II/III. GFP+ neurons deep layers in *Nprl3* KO specimens did not express CTIP2 indicating that these cells had failed to attain their appropriate laminar destination in layers II/III. GFP+ cells in layer II/III in *Nprl3* KO pups were larger than scramble cells in the layer II/III. Rapamycin treatment prevented laminar defects (A,B) and soma diameter increases (C; each box represents mean, S.E., whiskers represent 5-95% confidence intervals). (D), section from a surgical epilepsy FCD specimen (NeuN labeled, from a subject 18 in Fig. 1) shows heterotopic white matter neurons (arrows) similar to what was observed in mouse (A and E, arrows). (F). Five weeks after IUE, mice were implanted with dural EEG electrodes and recorded for 48 hrs. A representative line length analysis of the 48 hr. EEG recording shows increased line length (a proxy for spike amplitude) in the electroporated cortex suggesting a hyperexcitable cortex (n=6 per group) compared to the contralateral cortex and WT mouse cortices where line lengths in the right and left hemispheres were similar. Total average EEG power also showed increased power in *Nprl3* KO cortices compared to the contralateral cortex and control cortices (G). Rapamycin treatment after *Nprl3* KO rescued increased line length and EEG power (F, G). Mice were treated with 55 mg/kg PTZ and EEGs were recorded. (H), Representative EEG tracings in *Nprl3* KO, *Nprl3* +rapamycin, and WT mice. (I), After PTZ injection, *Nprl3* KO mice had a statistically significant average decrease (ANOVA; p<0.05) in latency to seizure (77.2 sec.) compared to WT mice (168 sec.). Rapamycin treated *Nprl3* KO mice had seizure latencies that did not differ from control mice (178 sec.). ***= p<0.001, *= p<0.05. Calibration mark in (A) = 200 µM.

Figure 6: Focal *Nprl3* KO *in vivo r*esults in increased PS6 levels. In (A) and (C) representative micrographs of 5-week-old *Nprl3* KO mouse brain and WT littermate control are shown, respectively. PS6 (240/244) levels were measure in GFP+ neurons (n=30 neurons per group). The dashed box in (A) demarcates the higher magnification area shown in (B). In (B), a GFP+ neuron (*triangle*) with increased

levels of PS6 (240/244) is shown in comparison to an adjacent neuron (*arrow*; not GFP+) with lower levels of PS6. Measuring the fluorescent intensity of PS6+ neurons revealed a statistically significant (ANOVA; $p < 0.001$) increase in PS6 levels in *Nprl3* KO neurons compared to non-GFP+ neurons located within the electroporated region and to neurons from WT littermates (D). In (D), boxes represents the SEM with a mean line shown, box whiskers represent the 5-95% confidence intervals. Total S6 levels were similar between Nprl3 KO and adjacent non-GFP+ neurons (Supplemental Figure 5). *** $p< 0.001$, calibration mark in (C)= 200 μm, calibration mark in (B) = 50 μm, AU = arbitrary units, adjacent= non-GFP+ neurons adjacent to GFP+ neurons.

Table 1 Summary of MRI and EEG findings in patients with *NPRL3* variants

Subject[a]	Age at EEG, years	MRI findings			EEG findings					
		Normal	HME	FCD	Normal	Focal/multifocal IED	Focal seizure	Focal slowing	Generalized IED	Generalized slowing
1	0			+		+	+	+		
2	0	+				+	+		+	+
3	1	+				+				+
4	1			+			+			
5	1			+		+	+	+	+	+
6	3			+		+	+	+		
7	4			+		+	+	+		
8	4			+		+	+	+		
9	6	+				+				
10	6		+			+		+	+	+
11	6	+				+	+	+		+
12	7	+				+	+	+		
13	8	–	–	–		+				
14	8			+		+		+		
15	9	–	–	–	+					
16	9	+					+			
17	11	+				+	+	+	+	+
18	15			+		+	+	+		
19	20	–	–	–	+					
20	21	+					+			+
21	31	–	–	–			+			

A plus symbol indicates presence on MRI or EEG. Dashes indicate no data were available.

[a]Subject numbers correspond to subject numbers in pedigree and MRI images in Fig. 1.

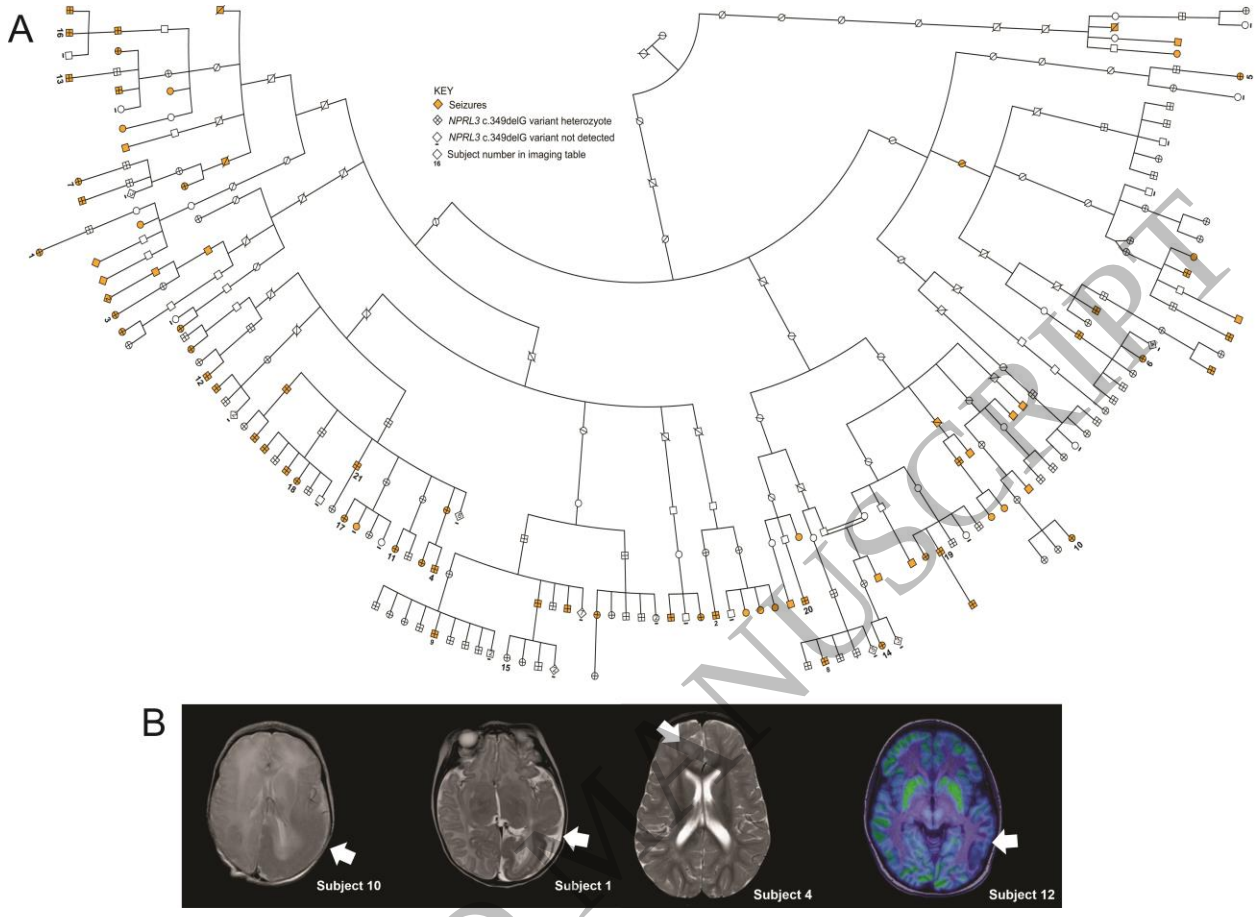

Figure 1
278x201 mm (6.5 x DPI)

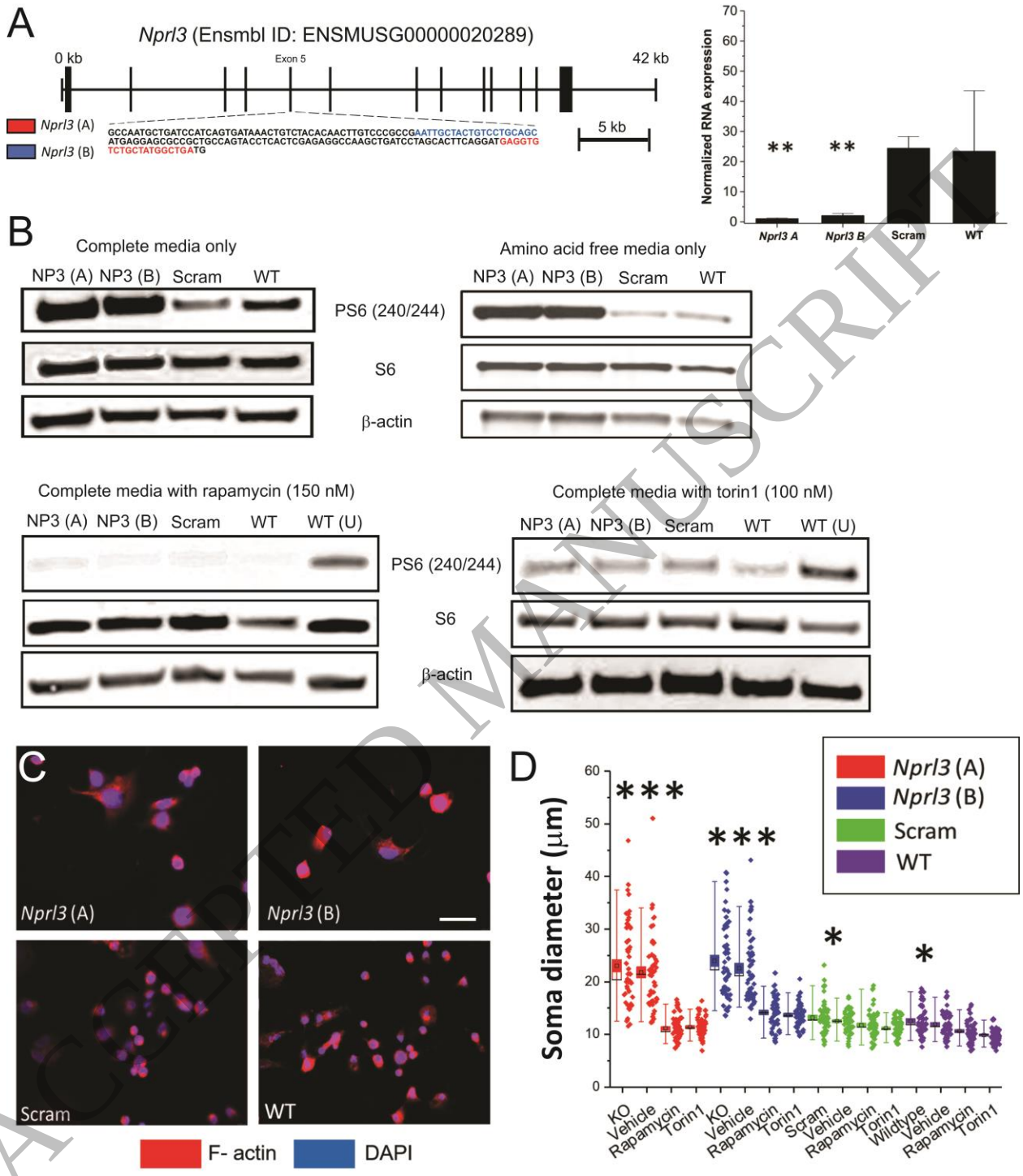

Figure 2
209x243 mm (6.5 x DPI)

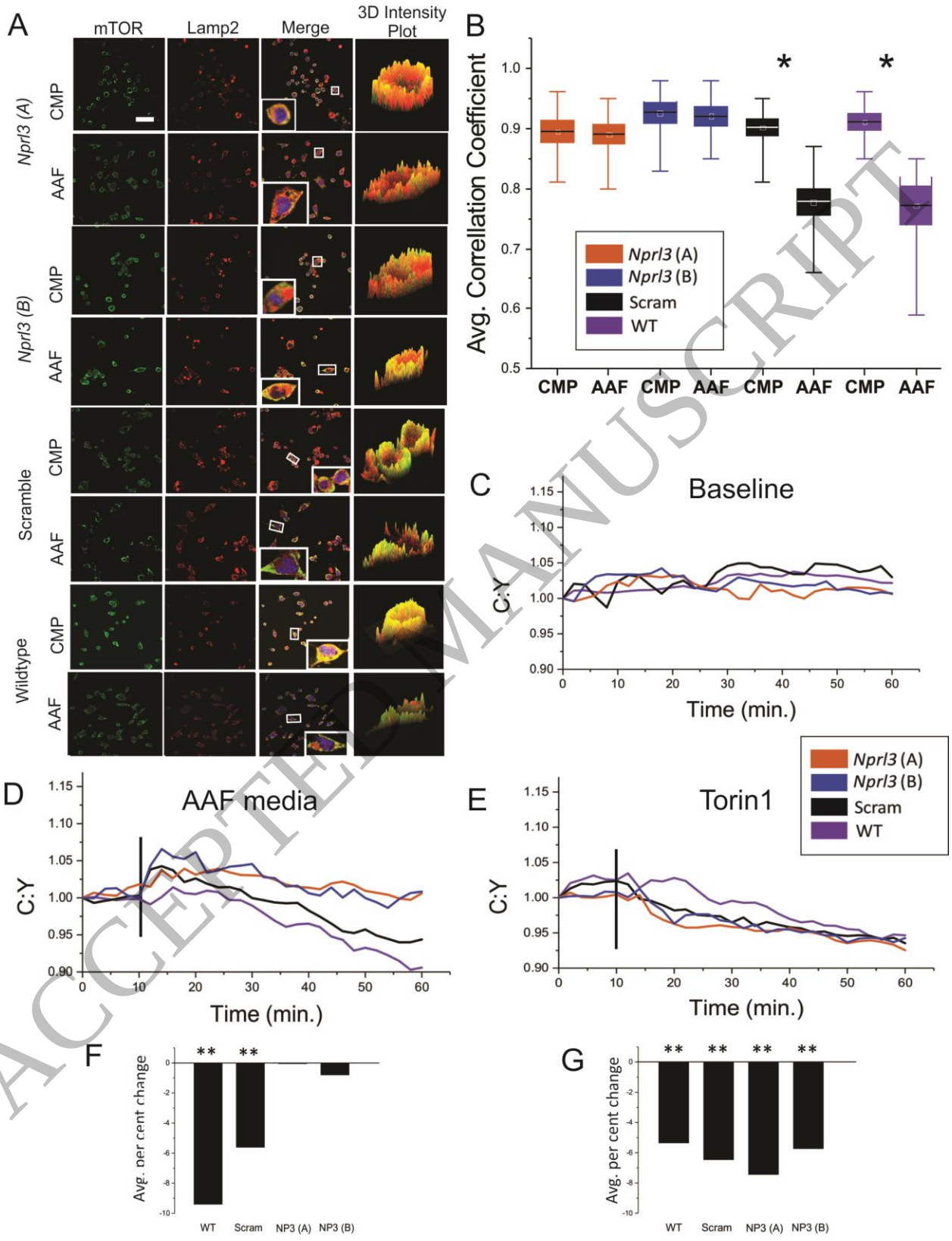

Figure 3
212x276 mm (6.5 x DPI)

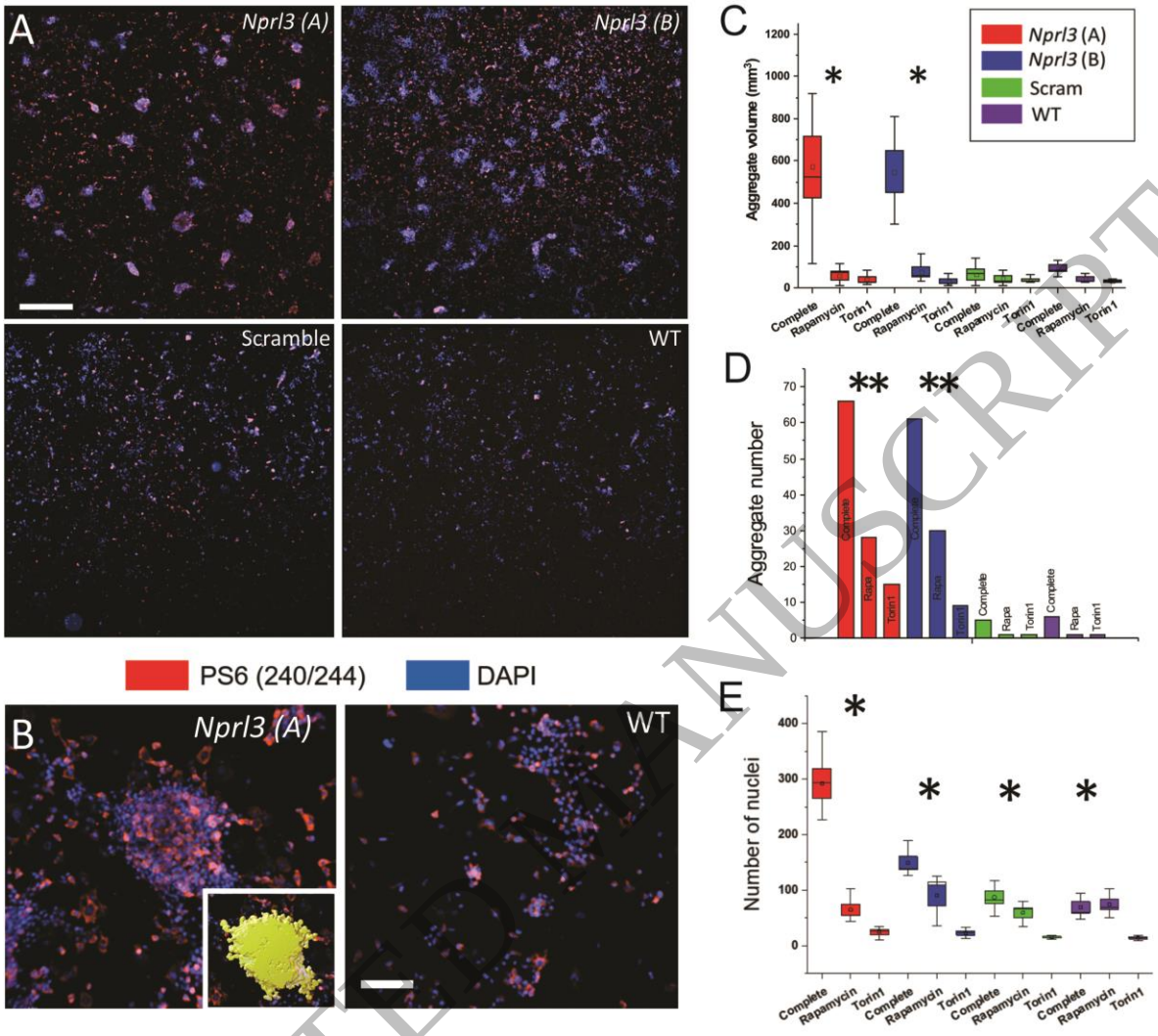

Figure 4
249x212 mm (6.5 x DPI)

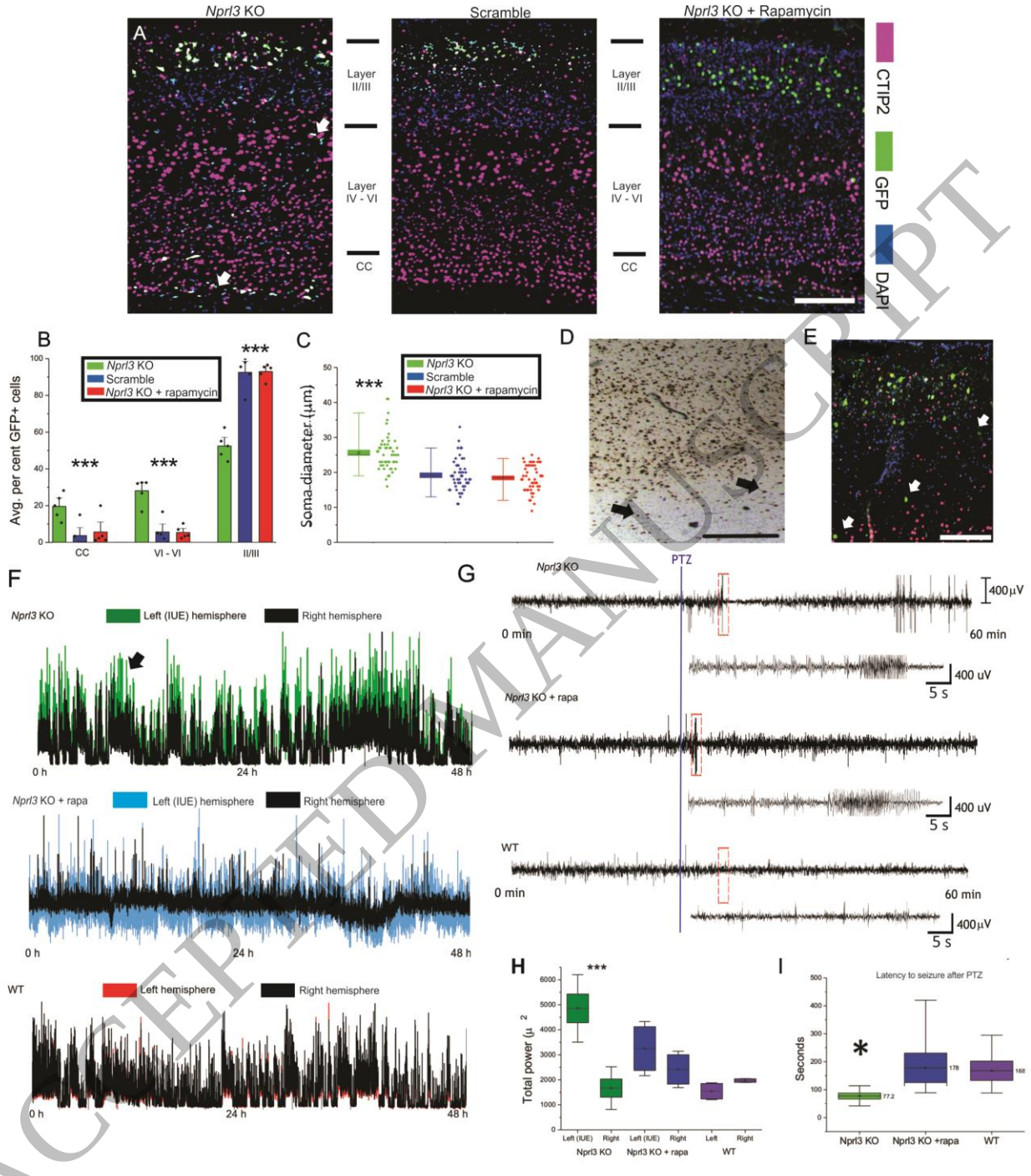

Figure 5
217x241 mm (6.5 x DPI)

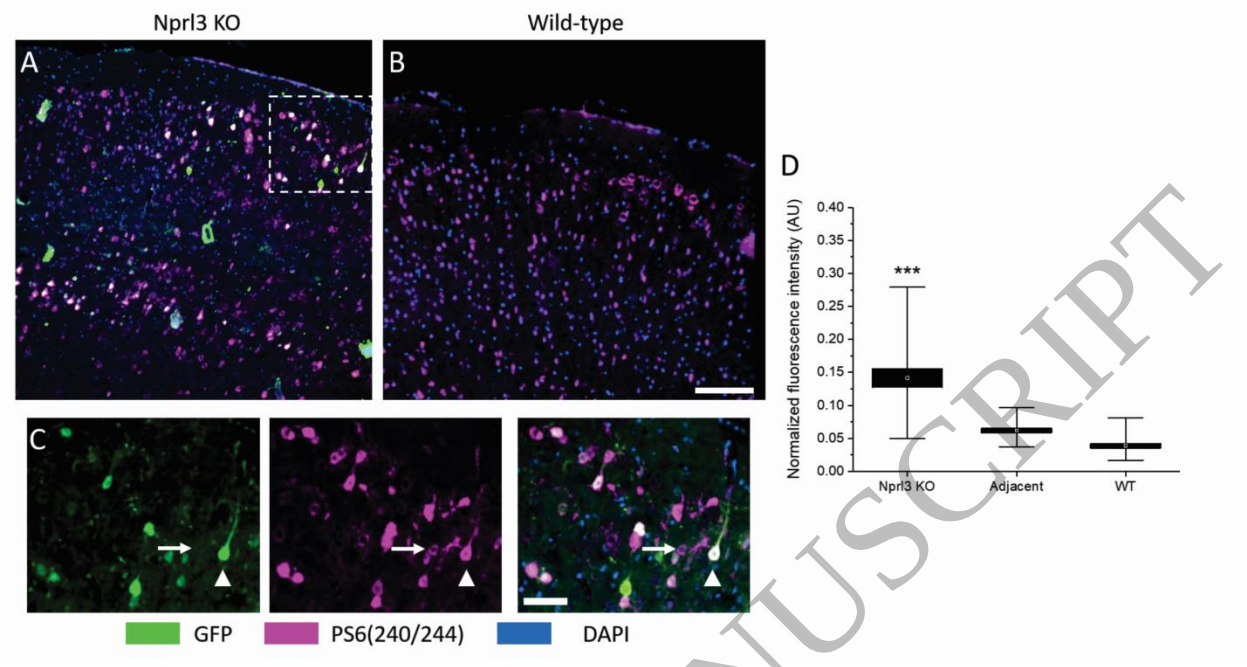

Figure 6
287x153 mm (6.5 x DPI)